Hybrid Silica/Polymer Aerogels Dried at Ambient Pressure

A. Fidalgo,[†] J. P. S. Farinha,[†] J. M. G. Martinho,[†] M. E. Rosa,[‡] and L. M. Ilharco*[,†]

Centro de Química-Física Molecular, Complexo I, and ICEMS (Instituto de Ciência e Engenharia de Materiais e Superfícies), Departamento Engenharia de Materiais, Instituto Superior Técnico, Av. Rovisco Pais, 1, 1049-001 Lisboa, Portugal

Received December 13, 2006. Revised Manuscript Received March 6, 2007

A novel sol−gel route was developed to prepare monolithic hybrid silica/polymer aerogels, stable under atmospheric conditions and suitable for machining. The synthesis of the hybrid wet gels followed a two-step hydrolysis/polycondensation of tetraethoxysilane with excess water, in 2-propanol. Cohydrolysis with trimethoxysilyl-modified poly(butyl metacrylate-*co*-butyl acrylate) cross-linked nanoparticles (average diameter of 94 nm) was carried out. Different alcogels were prepared varying the hydrolysis and condensation catalysis conditions and the polymer content (0−50% in weight). The aged alcogels were subcritically dried in a quasi-saturated solvent atmosphere. The resulting xerogels were characterized by dry-flow pycnometry, nitrogen adsorption−desorption, scanning electron microscopy (SEM), and diffuse reflectance infrared spectroscopy (DRIFT), and their mechanical properties were evaluated by unidirectional compression tests. The hybrid aerogels show improved mechanical properties with respect to the corresponding inorganic aerogel (much higher energy is stored until fracture), without loss of structure or porosity. The hybrid aerogels' properties are not monotonously dependent on the polymer content: the lowest density (357 $kg \cdot m^{-3}$) is achieved for 3 wt %, the corresponding porosity being 83%, the specific surface area 766 $m^2 \cdot g^{-1}$, and the average mesopore diameter 11.5 nm. This is also the most stable aerogel and the one with the best mechanical properties.

1. Introduction

Hybrid organic−inorganic materials are the result of an intimate mixture of organic and inorganic components. The organic/inorganic interactions may range from weak intermolecular, such as van der Waals or hydrogen bonds (in the so-called *class I* hybrid materials), to strong covalent or ionic−covalent bonds that prevent phase separation (in *class II* materials).[1] In either case, hybrid materials can be homogeneous or heterogeneous. The latter contain nanodomains of the two phases (currently described as nanocomposites) and thus the hybrid's physical, chemical, and mechanical properties depend not only on the individual components but also on the inner interfaces.[2,3]

The sol−gel process has emerged as the most successful method to synthesize hybrid organic−inorganic composites since the mild conditions involved in this soft chemistry process are ideal for avoiding damage to the organic components. The variety of inorganic and organic precursors available, as well as the multiplicity of strategies to the synthesis of hybrid sol−gel materials, broaden the range of structures and properties achievable and allow an impressive number of possible applications.[4,5] These include catalysis, optics, electronics, sensors, coatings, biochemistry, medicine, and others.[6−13]

A promising field to sol−gel hybrid inorganic−organic materials, namely, the silica-based ones, is thermal-acoustic insulation. Indeed, silica aerogels are known for their unique properties in this field: they are nonflammable, extremely light (densities in the range 3−500 $kg \cdot m^{-3}$), and excellent thermal and acoustic insulators (thermal conductivity in the range 0.01−0.02 $W\ m^{-1}\ K^{-1}$ and acoustic impedance between 103 and 106 $kg \cdot m^{-2} \cdot s^{-1}$).[14−18] The current drawbacks of these wonder materials are their high production costs, brittleness, and instability toward atmospheric moisture. Once their mechanical properties are improved and the production costs reduced, aerogels can become the insulators

* To whom correspondence should be addressed. E-mail: lilharco@ ist.utl.pt.
† Centro de Química-Física Molecular, Complexo I.
‡ ICEMS.

(1) Livage, J. *Curr. Opin. Solid State Mater. Sci.* **1997**, *2*, 132.
(2) Avnir, D. *Acc. Chem. Res.* **1995**, *28*, 328.
(3) Mackenzie, J. D.; Bescher, E. P. In *Handbook of Sol-Gel Science and Technology: Processing, Characterization and Applications*; Sakka, S., Ed.; Kluwer Academic Publishers: Boston, 2004.
(4) Nakanishi, K. *J. Porous Mater.* **1997**, *4*, 67.
(5) Sanchez, C.; Julián, B.; Belleville, P.; Popall, M. *J. Mater. Chem.* **2005**, *15*, 3559.
(6) Calvert, P.; Crockett, R. *Chem. Mater.* **1997**, *9*, 650.
(7) Schottner, G. *Chem. Mater.* **2001**, *13*, 3422.
(8) Lapidot, N.; Gans, O.; Biagini, F.; Sosonkin, L.; Rottman, C. *J. Sol−Gel Sci. Technol.* **2003**, *26* (1−3), 67.
(9) Houbertz, R.; Domann, G.; Schulz, J.; Olsowski, B.; Fröhlich, L.; Kim, W. S. *Appl. Phys. Lett.* **2004**, *84*, 1105.
(10) Fidalgo, A.; Ciriminna, R.; Ilharco, L. M.; Pagliaro, M. *Chem. Mater.* **2005**, *17* (26), 6686.
(11) Avnir, D.; Coradin, T.; Lev, O.; Livage, J. *J. Mater. Chem.* **2006**, *16* (11), 1013.
(12) Fesmire, J. E. *Cryogenics* **2006**, *46*, 111.
(13) Bardy, E.; Mollendorf, J.; Pendergast, D. *J. Phys. D: Appl. Phys.* **2006**, *39*, 1908.
(14) Hrubesh, L. W.; Tillotson, T. M.; Poco, J. F. In *Better Ceramics Through Chemistry*; Brinker, C. J., Clark, D. E., Ulrich, D. R., Zelinski, B. J., Eds.; Elsevier: New York, 1988.
(15) Fricke, J. *J. Non-Cryst. Solids* **1988**, *100*, 169.
(16) Gronauer, M.; Kadur, A.; Fricke, J. In *Aerogels*; Fricke, J., Ed.; Springer-Verlag: Berlin, 1986.
(17) Fricke, J.; Emmerling, A. *J. Am. Ceram. Soc.* **1992**, *75* (8), 2027.
(18) Fricke, J.; Gross, J. In *Chemical Processing of Ceramics I*; Lee, B. I.; Pope, E. J. A., Eds.; Marcel Dekker: New York, 1994; pp 311−336.

10.1021/cm062962w CCC: $37.00
Published on Web 04/24/2007

of the future. Organic−inorganic hybrids may have here a key role, and different approaches have been recently followed: crushed silica aerogels were embedded in binders;[19,20] fibers or high molecular weight polymers were either mechanically mixed with silica aerogel powder or added to the initial sol;[21−23] surface-modified silica aerogels were cross-linked with epoxides;[24] monolithic silica hydrogels were cross-linked with a diisocyanate solution (Desmodour N3200) and dried under ambient pressure.[25]

The present work aims at giving a contribution to this quest, profiting from the synergy of experiences existing in our team, in sol−gel, and in polymer chemistry, to produce monolithic hybrid silica/polymer aerogels, dried at ambient pressure, and stable under atmospheric conditions. Following extensive research on the design of pure silica xerogels, we have succeeded in synthesizing monoliths with densities as low as 350 kg·m^{-3}, with low hydrophilicity, and with tailored pore size distribution.[26,27] The synthesis consisted of a two-step process-acid hydrolysis of tetraethoxysilane (TEOS) followed by basic condensation under optimized catalysis conditions, controlled aging, and drying under a quasi-saturated solvent atmosphere. The main limitations to these materials were, probably, their fragility and the possibility of undergoing fatigue when submitted to cycles of mechanical efforts. To overcome them, TEOS was cohydrolyzed with functionalized core−shell polymer nanoparticles with low glass transition temperature (T_g), as shown in Scheme 1.

The polymer nanoparticles (PNP) are cross-linked, contain a low T_g trimethoxysilyl-modified poly(butyl metacrylate) [TMS−PBMA] shell, and an even lower T_g poly(butyl metacrylate-*co*-butyl acrylate) [P(BMA/BA)] core. Cross-linking stabilizes the spherical shape of PNP, allowing their dispersion in the sol−gel organic medium. The hydrolyzed TMS groups at the shell surface anchor the nanoparticles to the silica network, and the core−shell low T_g values contribute to the improvement in the mechanical properties of the hybrid material with respect to the inorganic aerogel.

2. Experimental Section

Scheme 2 illustrates the synthetic pathway to the hybrid silica/polymer xerogels.[28]

Scheme 1. Reaction Scheme to Obtain Class II SiO_2−PNP Hybrids[a]

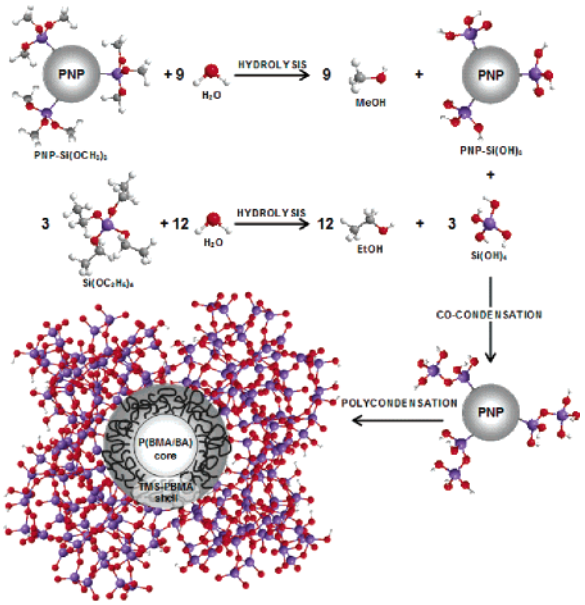

[a] Note: the size of PNP and its number of $Si(OCH_3)_3$ surface groups are only evocative of the real situation.

Scheme 2. Flow Diagram of the Hybrid Silica/Polymer Xerogels Synthesis Procedure

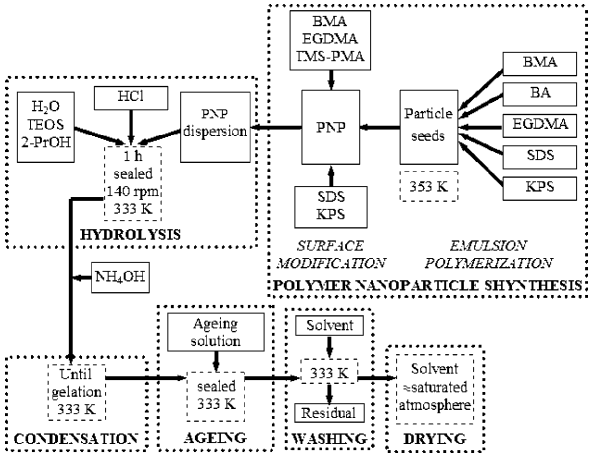

2.1. Synthesis of the Trimethoxysilyl-Modified Poly(butyl metacrylate-*co*-butyl acrylate) Cross-linked Core−Shell Nanoparticles. The synthesis of the core−shell polymer particles followed a two-stage emulsion polymerization technique. In the first stage, cross-linked seed particles (49 nm average diameter) were produced by batch emulsion polymerization. In the second stage, these seed particles were used to obtain cross-linked PNP (94 nm average diameter). The size and composition of the particles were controlled by a semicontinuous emulsion polymerization technique, with monomer and initiator fed under starving conditions.[29] The cross-linked seed particles were synthesized by copolymerization of *n*-butyl methacrylate (BMA, 99%) and *n*-butyl acrylate (BA, 99%), with ethylene glycol dimethacrylate (EGDMA, 98%) as cross-linker. The mixture was prepared in a glass reactor equipped with a condenser and a mechanical stirrer, emulsified with sodium dodecyl sulfate (SDS, 99%), and initiated with potassium persulfate (KPS, 99.99%). Phosphate buffer was used to maintain

(19) Kim, G. S.; Hyun, S. H. *J. Mater. Sci.* **2003**, *38* (9), 1961.
(20) Morris, C. A.; Anderson, M. L.; Stroud, R. M.; Merzbacher, C. I.; Rolison, D. R. *Science* **1999**, *284* (5414), 622.
(21) Martin, J.; Hosticka, B.; Lattimer, C.; Norris, P. M. *J. Non-Cryst. Solids* **2001**, *285* (1−3), 222.
(22) Zhang, Z. H.; Shen, J.; Ni, X. Y.; Wu, G. M.; Zhou, B.; Yang, M. X.; Gu, X. H.; Qian, M. J.; Wu, Y. H. *J. Macromol. Sci., Part A − Pure Appl. Chem.* **2006**, *43* (11), 1663.
(23) Frank, D.; Thönnessen, F.; Zimmermann, A. U.S. Patent 6,479,416 B1, dated Nov 12, 2006.
(24) Meador, M. A. B.; Fabrizio, E. F.; Ilhan, F.; Dass, A.; Zhang, G. H.; Vassilaras, P.; Johnston, J. C.; Leventis, N. *Chem. Mater.* **2005**, *17* (5), 1085.
(25) Leventis, N.; Palczer, A.; McCorkle, L.; Zhang, G.; Sotiriou-Leventis, C. *J. Sol-Gel Sci. Technol.* **2005**, *35*, 99.
(26) Fidalgo, A.; Rosa, M. E.; Ilharco, L. M. *Chem. Mater.* **2003**, *15*, 2186.
(27) Fidalgo, A.; Ilharco, L. M. *Microporous Mesoporous Mater.* **2005**, *84*, 229.
(28) Martinho, J. M. G.; Ilharco, L. M.; Farinha, J. P. S.; Fidalgo, A.; Martinho, P. O. Portuguese Patent PT-103257 and PCT-2006000010, April 5, 2005.
(29) Fonseca, T.; Relógio, P.; Martinho, J. M. G.; Farinha, J. P. S. *Langmuir* **2007**, in press.

pH = 7, by adding equivalent quantities of dihydrogenophosphate and dihydrogenocarbonate (typically 0.1 g of each per 100 g of water). The mixture was then purged with nitrogen gas for 2 h and heated to 353 K for an additional 2 h period. In a typical recipe, the reactor was filled with 95 wt % of water containing phosphate buffer, 4.5 wt % BMA, 0.4 wt % BA, 0.1 wt % EGDMA, 0.4 wt % SDS, and 0.1 wt % KPS. This produced a stable dispersion of particles with average diameter of 49 nm and narrow size distribution. In the second stage, the seed dispersion was purged with nitrogen for 15 min and heated to 353 K, under nitrogen. Two mixtures (one organic and one aqueous) were then independently fed into the reactor over 8 h, at constant rate, under stirring. The organic phase contained BMA, 3-(trimethoxysilyl)propyl methacrylate (TMS−PMA, 98%), and EGDMA. The aqueous phase contained phosphate buffer, SDS, and KPS. The reaction mixture was stirred at 353 K for an additional 2 h period before cooling to room temperature. In a typical recipe, 46 wt % of seed dispersion was added to 20 wt % BMA, 5.5 wt % TMS−PMA, and 1 wt % of EGDMA in the organic phase, and 0.4 wt % SDS, 0.03 wt % KPS, and ca. 27 wt % water in the aqueous phase. The particle growth was approximately linear (after a short initial induction time), as expected for starved feed in a system with high monomer conversion.[29] The synthesis yielded a 30 wt % solids stable dispersion of cross-linked core−shell particles with an average diameter (measured by dynamic light scattering) of 94 nm, and a narrow size distribution, showing that no aggregation takes place between the particles dispersed in water. The final particles have a trimethoxysilyl-modified poly(butyl metacrylate) shell and a poly(butyl metacrylate-*co*-butyl acrylate) core (TMS−PNP).

2.2. Preparation of the Hybrid Silica/Polymer Xerogels. The hybrid silica/polymer xerogels were synthesized by a two-step acid/base-catalyzed cohydrolysis/co-condensation of TEOS (98%) and TMS−PNP in 2-propanol (2-PrOH, p.a.), with a TEOS:H_2O:2-PrOH molar ratio of 1:4:9.2. The cohydrolysis reactions were triggered by the addition of hydrochloric acid (HCl, p.a.) 1 N to the initial mixture (water, TEOS, 2-PrOH, and TMS−PNP). The acidic sol was placed in a sealed container, heated at 333 K, and stirred for 1 h, to promote the cohydrolysis. The reaction mixture was then neutralized with ammonia (NH_4OH, p.a.) 0.1 N, promoting gelation by condensation of the pre-hydrolyzed species. The fresh alcogels were aged at 333 K, in sealed containers, for 48 h, the first 24 in the mother liquor and last in an aging medium containing water, TEOS, and 2-PrOH in the proportions used in the initial mixture. The aged alcogels were washed with 2-PrOH and subcritically dried, at 333 K, in a quasi-saturated solvent atmosphere, until negligible weight loss.[26] Following the above general procedure, the catalysis conditions were varied (HCl:TEOS and the NH_4OH:HCl molar ratios ranging from 3.0×10^{-3} to 7.0×10^{-3} and from 0.25 to 1.00, respectively), using a PNP content of 3 wt % (weight percent of the xerogel, roughly estimated assuming full conversion of TEOS into SiO_2). Hybrid silica/polymer xerogels with different PNP contents (ranging from 0.1 to 50 wt %) were prepared with HCl:TEOS = 7.0×10^{-3} and NH_4OH:HCl = 1.0. No phase separation was observed in any of the preparation steps.

2.3. Characterization. The hydrodynamic diameters of the polymer nanoparticles were obtained by dynamic light scattering, using Brookhaven Instruments (BI-200SM goniometer, 9000 AT-PCI autocorrelator, and APD detector) and a He−Ne laser (632.8 nm, 35 mW) from Spectra Physics model 127. The autocorrelation functions were analyzed with both Laplace inversion (CONTIN) and a sum of exponential functions (Expsam V3.0 programs included in the BI-ZP software package from Brookhaven). The envelope densities of the dried gels, degassed at room temperature prior to weighing, were determined by dry-flow pycnometery with a Micromeritics GeoPyc 1360, using a consolidation force of 50 N for 17 measurement cycles. The morphologies of fracture surfaces of the aerogels were characterized by scanning electron microscopy (SEM) with a Hitachi S4100-1, operating at 25 kV. The surfaces were previously sputter-coated with a gold layer ~20 nm thick, to avoid charging effects during observation. The pore structure was analyzed by N_2 adsorption−desorption isotherms at 77 K, with 10 s equilibration times, using a Micromeritics ASAP 2000. The samples were previously slowly degassed under vacuum: at 293 K for 24 h, and at 273 K for a further 24 h, to remove adsorbed compounds without causing partial densification of the material. The molecular structure of the aerogels was studied by infrared Fourier transform spectroscopy in diffuse reflectance mode (DRIFT), using a Mattson FTIR spectrometer with a Graseby Specac Selector, in the range 400−4000 cm^{-1}, with 4 cm^{-1} resolution. The mechanical properties of the xerogels were assessed by unidirectional compression tests. Cylindrical specimens were compressed along their axis, up to fracture, in a universal testing machine, SHIMADZU AG-5000, at 1.7×10^{-5} $m \cdot s^{-1}$ constant crosshead speed. The nominal strain rate, $\dot{\epsilon}$, obtained as the ratio of the crosshead speed to the initial height of the cylinder, varied between 1.0×10^{-3} and 3.0×10^{-3} s^{-1}. During the compression test, a load−crosshead displacement curve is recorded, which is then converted into a stress (σ)−strain (ϵ) curve, where stress is the ratio of the compression load to the initial cross section of the specimen, and strain is the ratio of the height decrease (crosshead displacement) to the initial height of the specimen.

3. Results and Discussion

3.1. Optimization of the Catalysis Conditions. Since both TEOS and the modifying TMS groups of PNP can undergo hydrolysis and condensation, with different reactivities, the catalytic conditions in each step of the acid/basic hydrolysis/condensation reactions are determinants of the hybrid xerogels physical properties, namely, their density and average pore diameter.

The hydrolysis pH was optimized by changing the HCl:TEOS molar ratio between 3.0×10^{-3} and 7.0×10^{-3}, while keeping the NH_4OH:HCl ratio at 1.0 (corresponding approximately to neutralization of the sol). HCl:TEOS molar ratios below 3.0×10^{-3} resulted in inorganic/organic phase separation, possibly due to hydrolysis and co-condensation of the TMS groups prior to TEOS hydrolysis, while molar ratios above 7.0×10^{-3} were responsible for a too fast gelation, leaving macroscopic solvent pockets within the alcogel, which jeopardized the integrity of the gel upon drying.

As can be seen in Figure 1A, the envelope density (ρ_e) consistently decreases from 753 to 357 kg m^{-3} with increasing HCl:TEOS molar ratio in the 3.0×10^{-3} to 7.0×10^{-3} range. This decrease is accompanied by an opposite variation of the average mesopore diameter (Φ) from 2.8 to 11.5 nm. These values were estimated from the corresponding N_2 isotherms (shown in Figure 2), by application of the Barrett−Joyner−Halenda (BJH) method to the desorption branch, assuming a cylindrical pore shape.[30]

With the HCl:TEOS molar ratio fixed at 7.0×10^{-3}, the catalytic conditions for condensation were optimized by

(30) Gregg, S. J.; Sing, K. S. W. *Adsorption, Surface Area and Porosity*, 2nd ed.; Academic Press: London, 1982.

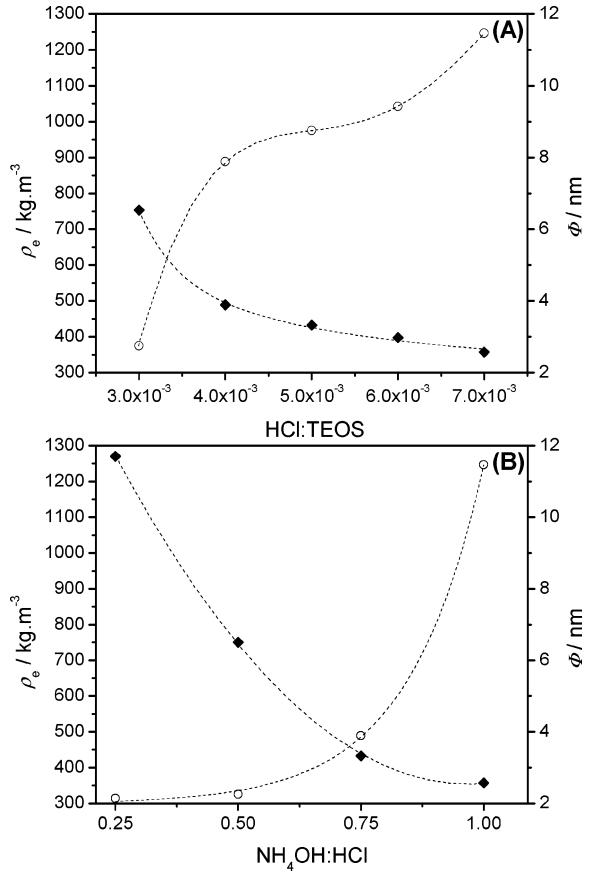

Figure 1. Envelope density (ρ_e, ◆) and average mesopore diameter (Φ, ○) of hybrid SiO_2/PNP (3 wt %) xerogels as a function of: (A) HCl:TEOS molar ratio, keeping NH_4OH:HCl = 1.0; (B) NH_4OH:HCl molar ratio, keeping HCl:TEOS = 7.0×10^{-3}.

varying the NH_4OH:HCl molar ratio between 0.25 and 1.0. Molar ratios below 0.25 produced very dense, microporous, brittle alcogels that fractured upon drying, while ratios above 1.0 were responsible for the formation of solvent pockets. As can be observed in Figure 1B, the increase in the NH_4OH:HCl molar ratio up to 1 (corresponding to a condensation pH of ~7) yields hybrid xerogels decreasingly dense, ρ_e varying from 1270 to 357 kg·m^{-3}. Simultaneously, the average mesopore diameters increase from 2.1 to 11.5 nm.

From the above results, it becomes clear that the minimization of the envelope density (via variation of the catalysis conditions) correlates with an increase of the average diameter of mesopores within the hybrid network. For HCl:TEOS and NH_4OH:HCl molar ratios above 0.006 and 0.75, respectively, the density of the hybrid materials obtained with 3 wt % polymer classifies them as aerogels.

The N_2 adsorption−desorption isotherms of the hybrid xerogels prepared under different catalysis conditions are shown in Figure 2 as a function of the HCl:TEOS (A) and NH_4OH:HCl (B) molar ratios.

All the hybrid xerogels prepared with different HCl:TEOS molar ratios present type IV isotherms, with hysteresis loops characteristic of capillary condensation in mesopores (Figure 2A). However, the change in the hysteresis type from H2 to H1 when the HCl:TEOS molar ratio is higher than 4.0×10^{-3} reveals a modification in the pore morphology: from a distribution of undefined pore shapes and sizes to a well-defined open-ended cylindrical pore network.[30−32]

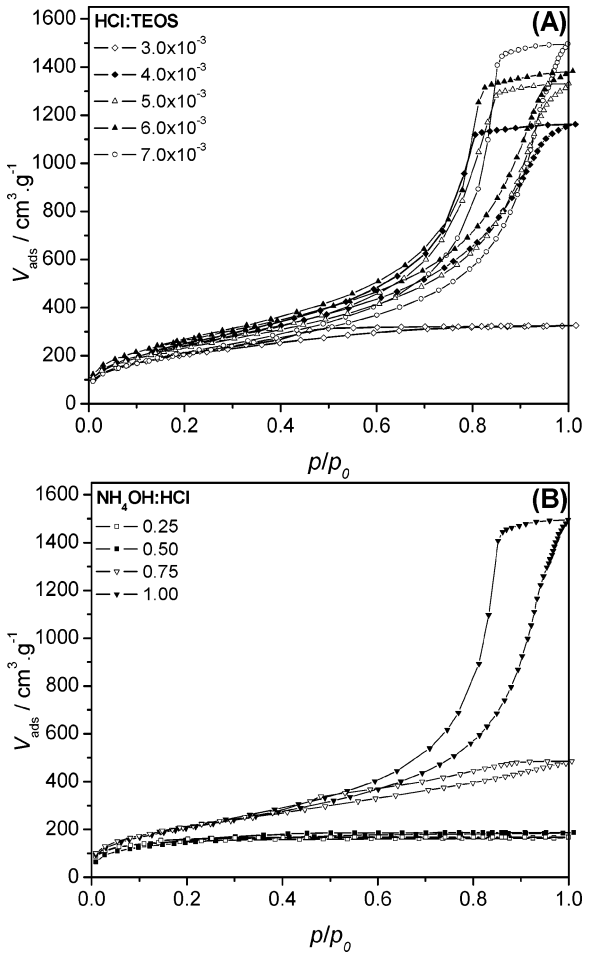

Figure 2. N_2 adsorption−desorption isotherms (at 77 K) of hybrid SiO_2/PNP (3 wt %) xerogels prepared with the following: (A) different hydrolysis catalytic conditions, keeping NH_4OH:HCl = 1.0; (B) different condensation catalytic conditions, keeping HCl:TEOS = 7.0×10^{-3}.

The hybrid samples prepared with a HCl:TEOS molar ratio of 7.0×10^{-3} and NH_4OH:HCl molar ratios below 0.5 exhibit type I N_2 isotherms, characteristic of microporous materials, but with some hysteresis, evidencing the coexistence of mesopores.[30] Above that NH_4OH:HCl molar ratio, type IV isotherms are obtained, the hysteresis loops changing from H2 to H1, when the ratio increases from 0.75 to 1.0.

The increase in the HCl:TEOS and NH_4OH:HCl molar ratios results in higher total pore volumes (calculated from $p/p_0 = 0.99$, roughly proportional to the plateaus of the isotherms) and is related to a modification of the material from micro-mesoporous (type I isotherms with hysteresis) to essentially mesoporous (with the characteristic type IV isotherms). The simultaneous increase in the average diameter of the network mesopores contributes to the reduction of the capillary pressure upon drying, preventing the collapse of the pores, and resulting in aerogel-like silica/polymer hybrid materials.[33,34]

3.2. Effect of the Polymer Content. Several hybrid samples were prepared with PNP contents ranging from 0.1

(31) Sing, K. S. W.; Everett, D. H.; Haul, R. A. W.; Moscou, L.; Pierotti, R. A.; Rouquérol, J.; Siemieniewska, T. *Pure Appl. Chem.* **1985**, *57*, 603.
(32) Ravikovitch, P. I.; Neimark, A. V. *J. Phys. Chem.* **2001**, *105*, 6817.
(33) Scherer, G. W. *J. Non-Cryst. Solids* **1987**, *89*, 217.
(34) Scherer, G. W. *J. Non-Cryst. Solids* **1992**, *147&148*, 363.

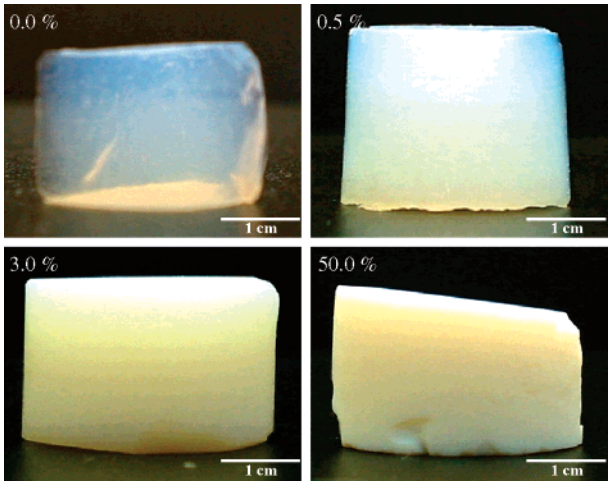

Figure 3. Photographs of slices of pure SiO_2 and three hybrid SiO_2/PNP aerogels with different polymer contents (weight percent as indicated).

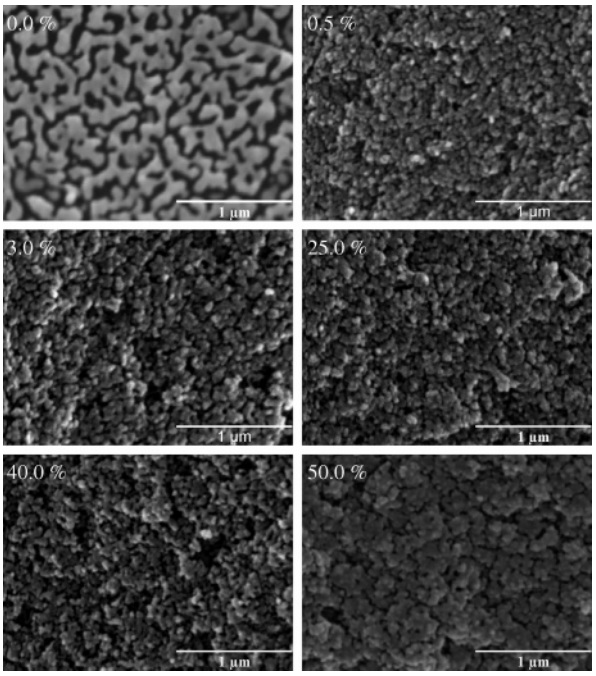

Figure 4. Cross-sectional SEM microphotographs of pure SiO_2 (0.0%) and hybrid SiO_2/PNP aerogels with different polymer contents.

to 50 wt %, using the optimized catalysis conditions for obtaining hybrid aerogels (HCl:TEOS and NH_4OH:HCl molar ratios of 7.0×10^{-3} and 1.0, respectively). Their properties were compared to those of an inorganic SiO_2 aerogel (corresponding to 0.0 wt % of polymer) prepared under the same catalysis conditions and following the same procedure as described in section 2.2.[26]

A macroscopic view of some selected hybrid samples is compared with that of pure SiO_2 in Figure 3. Upon drying, the transparent wet gels became either translucent (inorganic sample) or opaque (hybrid ones, even for very low polymer contents). Clearly, the presence of PNP in the structure increases the scattering. This can result from the modification of the pore network and/or from the scattering of the polymer particles.

The SEM microphotographs of fracture surfaces of these and other selected hybrid samples are shown in Figure 4.

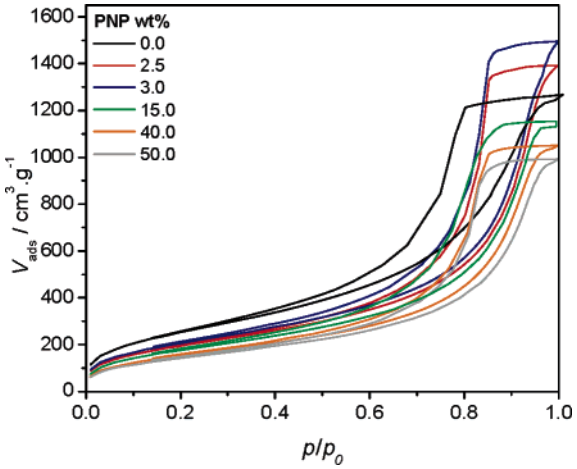

Figure 5. N_2 adsorption−desorption isotherms (at 77 K) of the inorganic and selected hybrid aerogels with different PNP contents.

All the samples show a bicontinuous distribution of interconnected particles and macropores, but it is clear that even a low polymer content (0.5 wt %) confers a drastic change to the xerogel's microstructure: it becomes more three-dimensional, with a more uniform distribution of smaller macropores. It appears that, due to the higher reactivity of TMS surface groups, PNP act as nucleation centers, conditioning the growth process of the silica network, irrespective of their content. As a result, a more branched, granular-like, structure is induced. Further modifications in the hybrid microstructure due to increasing the polymer percentage up to 40 wt % are not visible on this scale. For a 50 wt % polymer content, larger grains are observed, with apparently smaller macropores.

The effect of increasing the polymer content can be further elucidated by the xerogels' physical properties inferred from complementary characterization techniques.

The N_2 adsorption−desorption isotherms, shown in Figure 5, remain type IV over the entire range of polymer content. The hysteresis is clearly type H1 for all the samples, characteristic of a uniform distribution of cylindrical mesopores. However, for the inorganic aerogel the adsorption branch is not so steep, resulting in a broader hysteresis, which points to a less defined mesopore shape. The presence of PNP, irrespective of their content, seems to promote homogeneity in the aerogel's cylindrical pore network.

The plateau observed at high relative pressure (p/p_0) in the different curves clearly points to the existence of two distinct evolution trends: for low polymer contents (up to ~3 wt %), the total pore volume of the hybrid samples increases above that of the corresponding inorganic aerogel; higher polymer contents result in a decrease of the total pore volume, eventually reaching values below that of the inorganic sample.

The two evolution trends are well perceptible from the variation of the envelope density and the average mesopore diameter (estimated using the BJH algorithm, as described above) with the polymer content, illustrated in Figure 6, although the changes in these properties lie within narrow ranges. Up to ~3 wt % of PNP, the envelope density decreases (from 420 to 357 kg·m^{-3}) and the average mesopore diameter increases (from 8.4 to 11.5 nm); higher

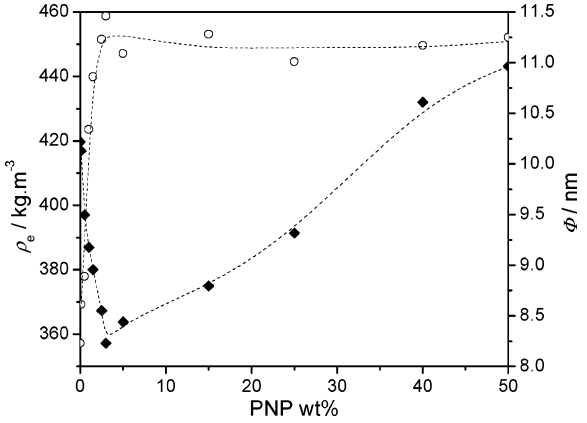

Figure 6. Variation of the envelope density (ρ_e, ◆) and average mesopore diameter (Φ, ○) with PNP content.

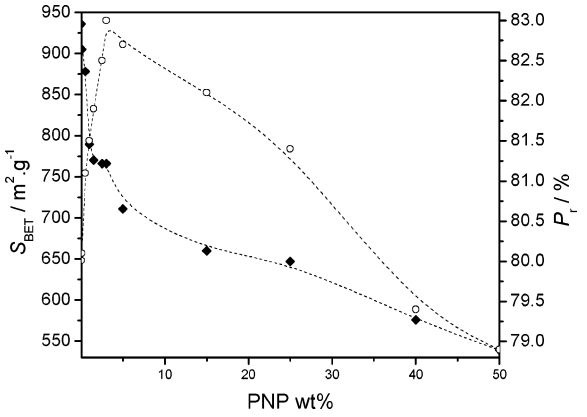

Figure 7. Variation of the specific surface area (S_{BET}, ◆) and percent porosity (P_r, ○) with PNP content.

polymer contents contribute to the increase in the envelope density (up to 443 kg·m^{-3} for 50 wt %), without variation of the average mesopore diameter.

The evolution of percent porosity (P_r) and specific surface area (S_{BET}) with PNP wt % is depicted in Figure 7. P_r was estimated from $100 \times (1 - \rho_e/\rho_s)$, taking the skeletal density, ρ_s, as 2100 kg·m^{-3} for all the samples.[35] S_{BET} was inferred from the N_2 sorption isotherms by a Brunauer−Emmett−Teller analysis of the amount of gas adsorbed at p/p_0 between 0.05 and 0.3, using N_2 cross-sectional area of 16.2 Å^2. [36]

While the percent porosity presents a maximum, reflecting the envelope density evolution, the specific surface area consistently decreases with increasing PNP content. However, once again, two distinct slopes may be observed: a steep one below 3 wt % PNP followed by a gentle one for higher contents.

From the above results, the following conclusions arise: a slight decrease in density (increase in porosity) may be achieved by synthesizing the aerogels with a small amount of PNP (up to ∼3 wt %). This is not due to an increase in macroporosity (which seems to decrease) but rather to the increase in the average dimensions of the mesopores, which acquire a more cylindrical shape. Consequently, the specific surface area decreases noticeably in this composition range. Above that polymer content, the size of mesopores stabilizes,

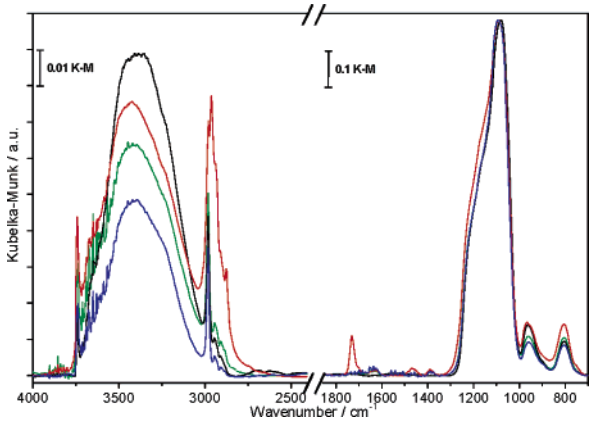

Figure 8. DRIFT spectra of selected aerogels with different PNP contents, normalized to the most intense band (at ∼1100 cm^{-1}): pure SiO_2 (black) and hybrid SiO_2/PNP aerogels containing 1.5 wt % (green), 3 wt % (blue), and 50 wt % (red) of polymer. The high wavenumber region is amplified ten times.

but the total porosity (macro plus meso) decreases, resulting in a more gentle decrease of the specific surface area with polymer content.

The hybrid materials were characterized, at the molecular structure level, by diffuse reflectance infrared spectroscopy. The spectra of some selected samples are shown in Figure 8. The spectral features are typical of a sol−gel silica network, with additional bands that grow with PNP content between 2981 and 2873 cm^{-1}, assigned to the polymer C−H stretching modes.[37] For high polymer contents (in Figure 8 only for the sample with 50 wt % PNP), other polymer bands become visible: at ∼1750 cm^{-1} (assigned to the carbonyl stretching mode), and between 1500 and 1300 cm^{-1} (assigned to the C−H deformation modes).[37] The weak and broad band centered at ∼3300 cm^{-1} is assigned to the stretching mode of O−H groups involved in different hydrogen-bonding interactions. They are mostly correlated with silanol (SiOH) groups since in these spectra there is no evidence of molecular water (in the H−O−H deformation region, at ∼1650 cm^{-1}, there is only water vapor miscancellation). Another silanol band, assigned to the Si−O(H) stretching mode, appears at 950 cm^{-1}. The strongest band, with maximum absorption at ∼1100 cm^{-1}, is assigned to the antisymmetric Si−O−Si stretching mode. The corresponding symmetric mode appears at ∼800 cm^{-1}. To allow a comparison of the bands evolution with respect to the silica network, the spectra were normalized to the most intense Si−O−Si band.

The low relative intensities of the silanol-related bands suggest an extensively condensed silica network. The subsequent absence of adsorbed water indicates that all the aerogels (even the inorganic) are poorly hydrophilic, and thus relatively stable under atmospheric conditions. The influnce of the polymer content on the relative intensities of the silanol-related bands suggests that the presence of PNP renders condensation more efficient, although increasing content above ∼3 wt % reduces its beneficial effect on the condensation yield. The ν_{as}Si−O−Si band is the most

(35) Woignier, T.; Phalippou, J. *J. Non-Cryst. Solids* **1987**, *93*, 17.
(36) Brunauer, S.; Emmett, P. H.; Teller, E. *J. Am. Chem. Soc.* **1938**, *60*, 309.
(37) Socrates, G. *Infrared and Raman Characteristic Group Frequencies*, 3rd ed.; John Wiley & Sons: New York, 2001.

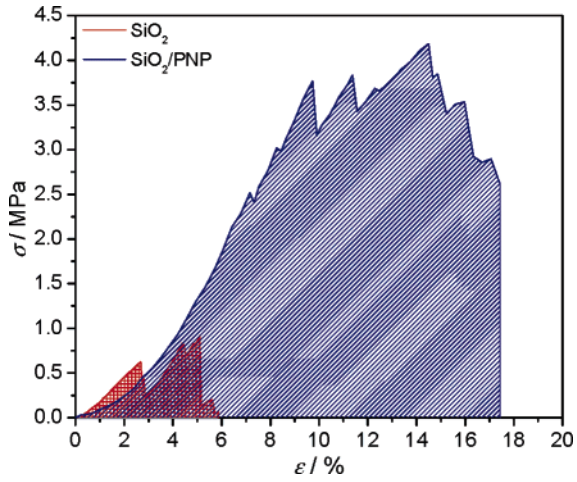

Figure 9. Stress−strain curves obtained from unidirectional compression tests of pure silica and a hybrid aerogel containing 3 wt % PNP.

informative on the structure of the silica network.[38] With the exception of the inorganic aerogel (shifted to lower wavenumbers) and the hybrid containing 50 wt % of polymer (broader), the spectra in this region are overlapped. A quantitative analysis of this band has been previously used to obtain detailed information on the dominant structural units that build the silica network, namely, $(Si-O)_4$ and $(Si-O)_6$ rings.[39] It has been shown that the relative proportions of these units correlate with the xerogel's percent porosity in the range 30−90%.[40] Since the samples in the present work have porosities within a narrow range (between 79 and 83%), it is expected that the structural units do not present significant variations, leading to similar profiles of the ν_{as}-Si−O−Si band. Once again, the silica structure is altered by the presence of PNP, but not significantly by its content, except when it reaches 50%.

Finally, the changes induced in the mechanical behavior of the silica aerogels by incorporation of PNP were evaluated by unidirectional compression tests. The stress−strain ($\sigma-\epsilon$) curves obtained for the pure silica and the 3 wt % PNP hybrid aerogels are compared in Figure 9.

Both curves present the typical features of brittle, cellular materials. The low-strain region corresponds to the reversible bending of the cells' walls, and the region with average lower slope relates to their buckling. The serrations along the compression curve result from successive fracture of the cells' walls. The region corresponding to general buckling and densification, where a slope re-increase would be observed, is absent.[41]

Table 1. Compression Properties of Pure Silica and 3 wt % PNP Containing Hybrid Aerogels

sample	E/MPa	σ_{max}/MPa	$\epsilon_{\text{"max"}}$/%
SiO_2	28	0.92	5.1
SiO_2/3 wt % PNP	44	4.24	14.4

The values of Young's modulus (E), the maximum compression strength (σ_{max}), and the corresponding strain ($\epsilon_{\text{"max"}}$) obtained from these curves are summarized in Table 1.

The brittle behavior of the silica aerogel remains upon the introduction of TMS-modified PNP. However, even a low polymer content promotes a clear improvement of the mechanical properties of the material: Young's modulus increases, and the maximum compression strength and the corresponding strain become 3−5 times higher. Furthermore, the mechanical behavior improvement is noticeable from the much higher energy that the hybrid aerogel is able to absorb up to the maximum compression strength (roughly the area under the $\sigma-\epsilon$ curve).

4. Conclusions

Nanostructured hybrid silica/polymer aerogels were successfully synthesized at ambient pressure as machineable monoliths, stable under atmospheric conditions. The hybrid aerogel with 3 wt % of polymer has a density of 357 $kg\cdot m^{-3}$, total porosity of 83%, average mesopore diameter of 11.5 nm, mechanical resistance to compression of 4.24 MPa, and maximum deformation of 14.4%. Such an amazing combination of properties makes these hybrid materials strong candidates for high-performance insulation applications.

Acknowledgment. This work was supported by Fundação para a Ciência e a Tecnologia (FCT), Projects POCTI/CEM/33487/2000 and POCTI/QUI/47885/2002. Alexandra Fidalgo acknowledges FCT for a post-doc grant (PRAXIS XXI/BPD/20234/2004). The authors wish to express their gratitude to Prof. Rui Almeida (DEM/IST) for the use of ASAP 2000 from Micromeritics.

CM062962W

(38) Fidalgo, A.; Ilharco, L. M. *J. Non-Cryst. Solids* **2001**, *283*, 144.
(39) Fidalgo, A.; Ilharco, L. M. *Chem. Eur. J.* **2004**, *10*, 392.
(40) Fidalgo, A.; Ilharco, L. M. *J. Non-Cryst. Solids* **2004**, *347*, 128.
(41) Gibson, L. J.; Ashby, M. F. *Cellular Solids: Structure and Properties*, 2nd ed.; Cambridge University Press: Cambridge, 1997.